# Influence of temperature fluctuations, measured by numerical simulations, on dust resuspension due to L.O.V.As

M.Benedetti, P.Gaudio, I.Lupelli, A.Malizia, M.T Porfiri, M.Richetta

***M.Benedetti*** is with University of Rome "Tor Vergata", Faculty of Engineering, Department of Mechanical Engineering, Quantum Electronics and Plasma Physics Research Group, Via del Politecnico 1, 00133 Rome, Italy (corresponding author phone: 0039 0672597196; fax: 0039 0672597207; e-mail: stilla_maris@hotmail.it).

***P.Gaudio*** is with University of Rome "Tor Vergata", Faculty of Engineering, Department of Mechanical Engineering, Quantum Electronics and Plasma Physics Research Group, Via del Politecnico 1, 00133 Rome, Italy (corresponding author phone: 0039 0672597209; fax: 0039 0672597207; e-mail: gaudio@ing.uniroma2.it).

***I.Lupelli*** is with University of Rome "Tor Vergata", Faculty of Engineering, Department of Mechanical Engineering, Quantum Electronics and Plasma Physics Research Group, Via del Politecnico 1, 00133 Rome, Italy (corresponding author phone: 0039 0672597196; fax: 0039 0672597207; e-mail: ivan.lupelli@uniroma2.it).

***A.Malizia*** is with University of Rome "Tor Vergata", Faculty of Engineering, Department of Mechanical Engineering, Quantum Electronics and Plasma Physics Research Group, Via del Politecnico 1, 00133 Rome, Italy (corresponding author phone: 0039 0672597196; fax: 0039 0672597207; e-mail: malizia@ing.uniroma2.it).

***M.T. Porfiri*** is with ENEA FUS-TEC (Fusion Safety & Environment) Via Enrico Fermi, 45, 00044 Frascati (Roma), Italy. (corresponding author phone: 0039 0694002654; e-mail: maria_teresa.porfiri@enea.it).

***M.Richetta*** is with University of Rome "Tor Vergata", Faculty of Engineering, Department of Mechanical Engineering, Quantum Electronics and Plasma Physics Research Group, Via del Politecnico 1, 00133 Rome, Italy (corresponding author phone: 0039 0672597197; fax: 0039 0672597207; e-mail: richetta@uniroma2.it).

*Abstract*
ITER will be the first challenge to demonstrating licensable fusion safety and environmental potential of fusion and thereby provide a good precedent for the safety of future fusion power reactors. In next step devices, dust will play an important role in determining their safety and operational performance. By the nature of its operation, a Tokamak generates aerosol particulate, broken flakes, globules, chunks, and other debris, that may affect its safety and operational performance so nuclear fusion safety field requires the development of specific codes or additional validation of existing ones to deal with all fusion specific conditions (typical temperature ranges of the plants, the potential use of specific cooling fluids, high flux of highly energetic neutrons, large amount of tritium and dust, the use of specific materials like W, Be, V).
This work is intended to contribute towards improving the understanding of processes taking place during air LOVA. The simulation of LOVA scenario is a challenging task for today numerical methods and models because it involves three dimensional geometry with large volume. The research activity has been carried out in the framework of EURATOM-Quantum Electronics and Plasma Physics group of University of Rome "Tor Vergata" and ENEA Fusion Technology Department at Frascati National Laboratory.
Numerical simulation and experimental activities have been carried out in strong correlation in order both to understand the capabilities of computational codes and to predict correctly the characteristics of the flows during a LOVA event. Obtained results are compared to experimental data provided by STARDUST facility. STARDUST facility is selected both for the model development phase and validation case.
The adopted code should has the capability to treat the main physical phenomena occurring during a LOVA event in particular the authors will present the results related to the influence of temperature variations.

***Keywords*** — ITER; Velocity; Temperature; Simulation; LOVA; Pressurization rate ; STARDUST.

## I. Introduction

This work takes ITER as reference machine because it is the most interesting project in the fusion safety field for its safety concerns and lay out. Nevertheless the results are not straight applicable to the international fusion reactor. The study was developed on the frame of the computer code validation for nuclear safety accident analysis. It is a starting point for dust mobilization investigation but it needs large verification before being extrapolated to facilities bigger than STARDUST.

Intense thermal loads in fusion devices occur during plasma disruptions, Edge Localized Modes (ELM) and Vertical Displacement Events (VDE). They will result in macroscopic erosion of the plasma facing materials and consequent accumulation of activated dust in Vacuum Vessel (VV). In ITER it is foreseen that the continuous first wall erosion caused by plasma disruptions and the bumps of the plasma during the operation induce the formation of mobilizable materials, in shape of radioactive dust [1]. The safety limit for dust inside the ITER Vacuum Vessel (VV) has been proposed to the safety authorities to be 1000 kg, without any precision on the composition. However, it is settled also a "hot dust" limit (defined as the dust on surfaces with T>400°C) of 6 kg each of C, Be and W [2]. These administrative limits have been fixed to avoid, also in case of severe accident, the evacuation of the population from the area surrounding the plant [2] because the consequent calculated releases should cause doses below the limits according the current recommendations of the International Commission on

Radiological Protection. In case of LOVA [3], air inlet occurs due to the pressure difference between the atmospheric condition and the internal condition. A LOVA event causes mobilization of the dust that can exit the VV, threatening public safety because it contains tritium, it is radioactive from activation products, and may be chemically reactive and/or toxic [1]. Several experiments with STARDUST facility have been conducted to reproduce a low pressurization rates LOVA [3] event in ITER due to a small air leakage for one position of the leak, at the equatorial port level in order to evaluate the influence of flow field and temperature on dust resuspension. The pressurization rate of 300 Pa/s is the estimated consequence of a 0,02 $m^2$ wide breach during the first seconds of a LOVA, as defined by Generic Site Specific Report (GSSR) [4].In these work have been considered different flow rates in order to evaluate the effects due to several accidental conditions. The authors will present and discuss experimental evidences and results in order to put in evidence the criticism of every accidental conditions.

## II. STARDUST

STARDUST (Figure1) is a small facility, set up in the ENEA laboratories of Frascati (by Fusion Technology Department) in collaboration with the Research group of Quantum Electronics and Plasma Physics of University of Rome "Tor Vergata" and represents a section, in scale, of ITER Vacuum Vessel.
STARDUST is a stainless steel tank with a cylindrical shape in made to reproduce LOVAs and analyze the behavior of dust due to these accidents.[5]
The functional scheme of STARDUST is showed in figure.1.

**Fig. 1** *STARDUST*

In STARDUST the main objective is to reproduce LOVAs as those expected in ITER for sealing failures (for example) and to obtain, by means of the comparison among experimental and numerical data, the basis for a mathematical model suitable to simulate dust behavior in such accidents. [5,6,7]
The main geometrical features of STARDUST facility are showed in the table that follows (Tab.1):

| | |
|---|---|
| External length of the tank (mm) | 920 |
| External diameter of the tank (mm) | 506 |
| External diameter of the lids (mm) | 570 |
| Thickness of the tank's wall (mm) | 5 |
| Thickness of the lid (mm) | 14 |
| Quartz lateral windows : distance from the pipe inlet (center of the window) (mm) | 182 |
| Diameter of the lateral quartz windows (mm) | 84 |
| Diameter of the frontal quartz window in the mobile lid (mm) | 79 |
| Internal volume of the tank (m3) | 0,17 |

**Tab.1** *STARDUST geometrical features*

Now the Labview software to manage hardware and acquire data will be briefly explained in order to understand how is possible reproduce LOVA with STARDUST.

1. The program asks to the user to switch on the heaters that regulate the electrical resistances wrapped around STARDUST wall (for warm experiments, at walls temperature of 120-130 °C), in case of cold experiments (environmental temperature) the heaters will not be switched on;
2. The pneumatic-valve relay is automatically activated and the valve is open;
3. The program reminds the user to open the vacuum valve;
4. Now the achievement of boundary condition is started, and the user can monitor the temperature and pressure conditions and the values of flow rate trough the flow meter by the display showed in figure 22 and automatically open by the program (this display takes data by the input cards and show it in continuum mode).
5. When the boundary conditions are reached ($P_{internal}$=100 Pa or 1000 Pa and T = 25°C (cold experiments) and T=120-130 °C (hot experiments)) the program automatically closes the pneumatic-valve stopping the air extraction by vacuum pump;
6. The program asks to the users the valve used (A) and the path-file for the data storage;
7. Automatically feed valve is opened (by external relay controlled by internal relay by the program) and by the analogical output card a voltage signal is sent to the flow meter to activate the air compressed flowing trough valve A. The air flows with a pressurization rate of 100Pa/s or 300 Pa/s or 500 Pa/s, obtained with the flow rates showed in table 2;

| Temperature | Pressurization rate | Flow rate |
|---|---|---|
| Environmental | 100 Pa/s | 8 lt/min |
| | 300 Pa/s | 22 lt/min |
| | 500 Pa/s | 41 lt/min |
| 120-130 °C | 100 Pa/s | 10 lt/min |
| | 300 Pa/s | 26,5 lt/min |
| | 500 Pa/s | 52 lt/min |

**Tab. 2:** *Flow rate setting*

In order to measure all the parameters inside STARDUST are placed :

i. *For internal pressure measurements:* Three pressure gauges placed on [5,6,7] the top of STARDUST (as showed in Fig. 2):
   - Leybold Heareus Barometer;
   - BOC EDWARDS ASG-2000-NW16 pressure gauge;
   - Alcatel AP 1004 Pirani.

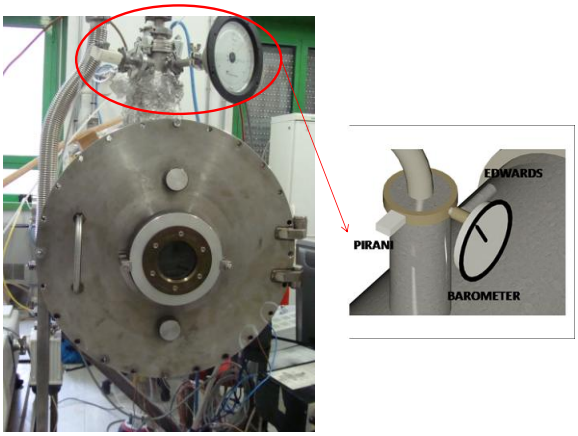


**Fig.2**: *Pressure gauges positions*

ii. *For temperature measurements:* four thermocouples J type

iii. *For velocity measurements:* Two XCE-093-2D [8,9,10] Kulite pressure transducers (after called PT 455 and PT 461) that area pressure detector realized with a monolithic piezo-resistive sensor in silicon that works in a temperature range from -55 to 273 °C, even if the pressure transducer operations are optimized for the temperature range from 25 °C to 235 °C (and it allows the measurements in our experimental conditions).

The velocity values are obtained by an empirical equations that follows [6]:

$$v = \sqrt{\frac{2\gamma R\overline{T}}{M(\gamma-1)}\left[\left(\frac{P_\Delta + P_s}{P_s}\right)^{\frac{\gamma-1}{\gamma}} - 1\right]}$$

Where:

- $\gamma$ : ratio of the fluid specific heat at constant pressure to the fluid specific heat at constant volume ($c_p/c_v$) and is approximately *1.4* for air;
- **R** : universal gas constant (8,314 J $K^{-1}$ $mol^{-1}$ ) ;
- $\overline{T}$ : mean temperature ;
- **M :** air molecular mass (28,968 g/mol);
- $\mathbf{P_s}$ : static pressure ;
- $\mathbf{P_\Delta}$: differential pressure ($P_\Delta = P_T - P_s$).
- $\mathbf{P_T}$ : total pressure

8. Immediately after the flow rate activation (the time depends by time machine time) the acquisition starts, and the data are stored in a file (with a frequency of 50 Hz) in the following order :
   a. Acquisition number;
   b. Pressure transducer value (PT455);
   c. Pressure transducer value (PT461);
   d. Pressure transducer value (PT464);
   e. Pressure value;
   f. Temperature value of thermocouple n°2;
   g. Temperature value of thermocouple n°3;
   h. Temperature value of thermocouple n°4;
   i. Flow rate value.

When the internal pressure of 95000 Pa is achieved the program automatically allows the closure of flow meter and the experiment is over. After these data acquisition, by a MATLAB software, all data are elaborated in order to obtain velocity values and velocity errors.

## III. Experimental set-up

In the previous sections has been explained how it is possible to reproduce a LOVA with STARDUST. The STARDUST set up has been used to make experimental campaigns.

*Experimental scheme*: Velocity mapping in STARDUST during a LOVA reproduction, trough valve A under the experimental conditions showed in table 2 and following the experimental path showed in Figure 3;

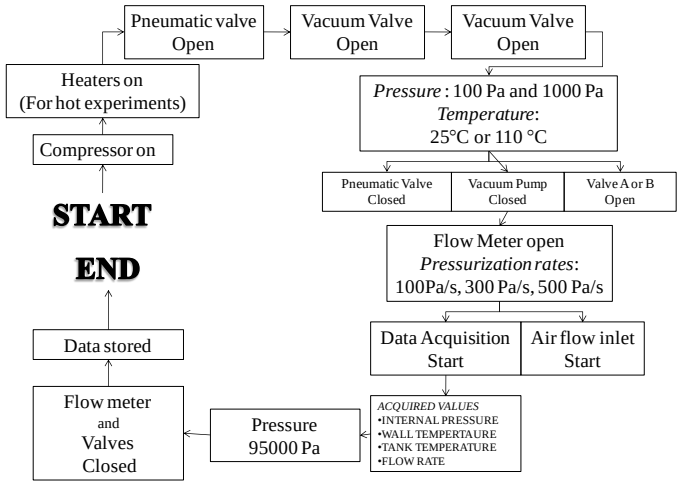


**Fig.3**: *STARDUST functional scheme for LOVA reproduction*

In the following section the experimental setup for experimental campaign will be explained.
To map the velocity flow values in the tank the sensor has been placed inside a circular support system (Fig.4) that has been placed in several sections of the tank to obtain a velocity mapping.

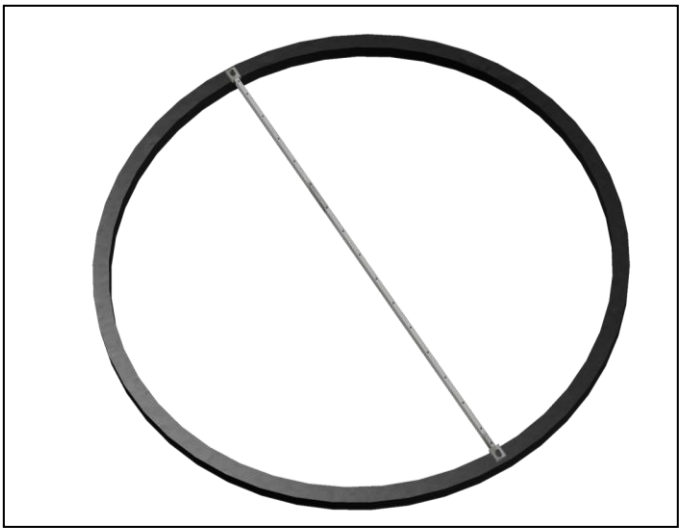

**Fig.4**: *Pressure transducer support*

The support has been positioned at several distances from the valves air inlet positions

- 4 cm;
- 22,75b cm;
- 45,5 cm
- 68,25 cm.

The pressure transducers are placed inside the tank, on these support, on the points reported on table 3 and figure 5.

| Probe Coordinates | | | | |
|---|---|---|---|---|
| Name | Plane | x[m] | y[m] | z[m] |
| A | Equatorial | 0,01 | 0,248 | 0 |
| B | | 0,2275 | 0,248 | 0 |
| C | | 0,455 | 0,248 | 0 |
| D | | 0,6825 | 0,248 | 0 |
| E | | 0,6825 | 0,248 | -0,243 |
| F | | 0,455 | 0,248 | -0,243 |
| G | | 0,2275 | 0,248 | -0,243 |
| H | Symmetry | 0,01 | 0,486 | 0 |
| I | | 0,2275 | 0,486 | 0 |
| L | | 0,455 | 0,486 | 0 |
| M | | 0,6825 | 0,486 | 0 |
| N | | 0,6825 | 0,0095 | 0 |
| O | | 0,455 | 0,0095 | 0 |
| P | | 0,2275 | 0,0095 | 0 |
| Q | | 0,01 | 0,0095 | 0 |
| **Directions** | | | | |
| **Name** | **Plane** | **Point** | | |
| Line 1 | Equatorial | B-G | | |
| Line 2 | | C-F | | |
| Line 3 | | D-E | | |
| Line 4 | Symmetry | H-Q | | |
| Line 5 | | I-P | | |
| Line 6 | | L-O | | |
| Line 7 | | M-N | | |

**Tab. 3** *Pressure transducers positions*

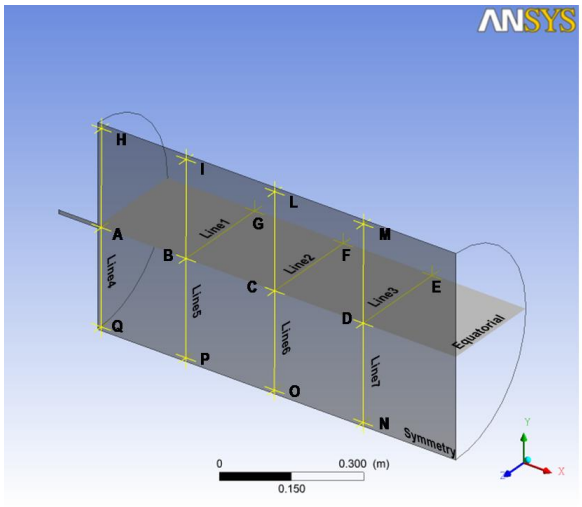


**Fig.5** *Pressure transducer scheme*

The pressure transducer 455 has been placed on points A,B,C,D with the sensible element on the valve A (facing the flow field air flux) as in figure 6 that represents the verse of transducers on line I-P positions B (PT 455), and P (PT 461).

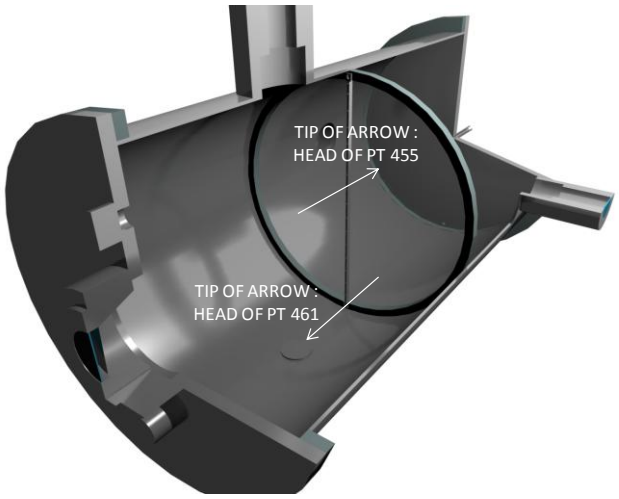


**Fig.6** *Versus of PTs*

The pressure transducer 461 has been placed on the other points (by rotating the support) with the sensible element on the lid (facing the flow field air re-flux).

For each positions the experiments have been repeated for each of the configuration reported in table 2, in both maintenance conditions ($T_{walls}$ : 25 °C) and operative conditions ($T_{walls}$ : 120-130 °C) and with both the initial pressure conditions considered (100 Pa and 1000 Pa).

All the parameters are stored and in few seconds, when the internal pressure equals the external ones, the acquisition stop and a file.dat is stored with all the parameters showed before.

## IV. Experimental Results

The previous experimental campaigns and numerical simulations [9,10] have put in evidence that the first 3-4 seconds are the most important for dust resuspension in case of LOVA (almost all dust resuspendend in these seconds).
In these period the mean temperature for hot experiments and cold experiments doesn't change substantially (in Fig. 7 is showed the mean temperature in the first 5 second for a cold experiment with an initial pressure of 100 Pa and a pressurization rate of 100 Pa/s).

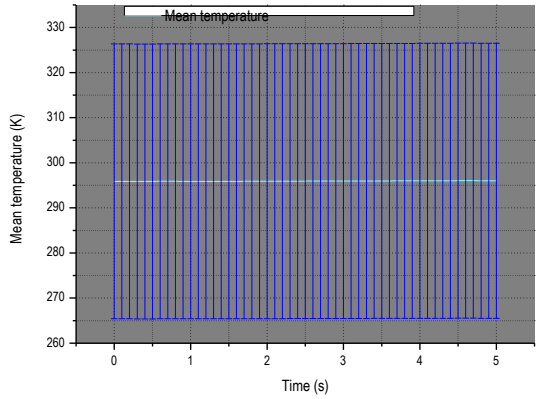


**Fig.7** *Mean Temperature 100Pa_100Pa/s_cold experiment*

The other experimental evidence is that the flow rate has been changed in order to obtain the pressurization rates (100 Pa/s, 300 Pa/s and 500 Pa/s) to simulate different LOVAs.
By passing from experiments with wall temperature of 120-130 °C to 25 °C (Tab. 2) is it possible observe that the flow rate has to be reduced of 20% to obtain the same pressurization rate.
The velocity flow field for every single point of Fig. 5 has measured for each of the experimental set-up. In the figure that follows (Fig. 8 ) there is the graph of velocity for the first 5 seconds.

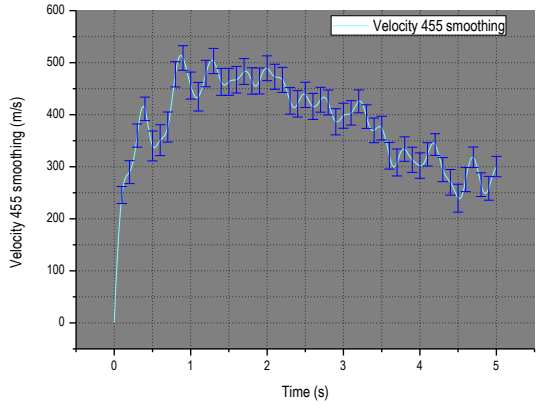


**Fig.8** *Mean Temperature 100Pa_100Pa/s_cold experiment*

After the analysis of all the experimental data, the comparison of maximum velocity values measured by the pressure transducer placed as figure 6 in different point on the same lines. The figures that follows (Fig.9 and Fig.10) shows a comparison between velocity values measured (with an initial pressure of 100 Pa, a pressurization rate of 100 Pa/s and Twall=25 °C) on:

- the central line by PT 455 (Points : A-B-C-D) (Fig. 9);

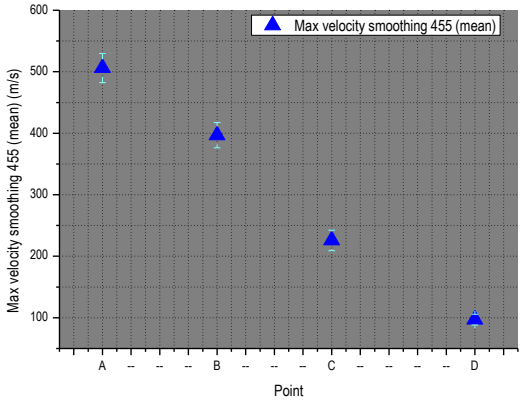


**Fig.9** *Velocity comparison at 100Pa_100Pa/s_cold experiment for central line*

- the inferior line by PT 461 (Points : Q-P-O-N) (Fig.10);

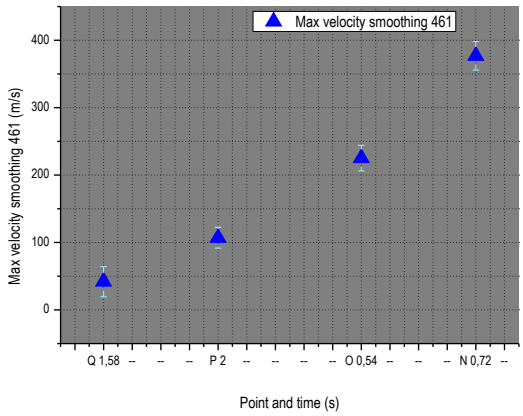


**Fig.10** *Velocity comparison at 100Pa_100Pa/s_cold experiment for inferior line*

## V. Numerical Simulations

Within the future safety problems related to nuclear fusion plants, several safety related simulation codes are currently used for demonstrating the safe behavior of the concerned machine and the limited impact on the population and environment in various situations from the normal operation up to the largest credible accident. These codes are ranging from neutronics calculation and dose assessment to the modeling of accident sequences and thermo hydraulics analysis in normal, incidental and accidental situations (Massaut). The present section is focused on the development of the CFD model of the LOVA. It is expected that it can be used to address the phenomenological questions of the LOVA

that will result as part of the licensing of future nuclear fusion reactor without conservative assumptions in analysis.

V.I INTRODUCTION

The ANSYS CFX solver uses finite elements (cell vertex numerics) to discretize the domain. Supersonic flow that occurs in a LOVA event during the expansion of a jet into vacuum condition are, in general, more difficult to solve than subsonic or incompressible flow problems. This is due to the highly non-linear nature of supersonic flows, especially when shocks are present. The advection terms in govern equation, accounting for the wave propagation phenomena and the presence of discontinuities in transonic and supersonic flows, are modeled by upwind methods. Upwind schemes use an adaptive or solution-sensitive finite difference stencil to numerically simulate more properly the direction of propagation of information in a flow field. ANSYS CFX focuses on one approach to solve the governing equations of motion following the implicit pressure based coupled algebraic multigrid approach. This technique solves the fluid-dynamic equations (for u, v, w, p) as a single system. Segregated solvers employ a solution strategy where the momentum equations are first solved, using a guessed pressure and an equation for a pressure correction is obtained. Because of the guess-and-correct nature of the linear system, a large number of iterations are typically required in addition to the need for selecting relaxation parameters for the variables.

V.II GOVERNING EQUATIONS

In this section governing equation are presented (Bodi, 2005). The governing equation are applied to an infinitesimally small control volume located in a moving fluid. This application results in partial differential equations (PDEs) formulation. The set of governing equations can be cast as a single equation called the transport (for a Newtonian fluid are named Navier-Stokes equations (NSEs) equation for property (or generic field) Φ:

$$\underbrace{\frac{\partial(\rho_m \Phi)}{\partial t}}_{\substack{\text{Rate of change}\\ \text{the amount}\\ \text{of extensive property}\\ \text{in the control volume}}} + \underbrace{\frac{\partial\left(\rho_m u_j \Phi\right)}{\partial x_j}}_{\text{Convection term}} = \underbrace{\frac{\partial}{\partial x_j}\left[\Gamma_{eff}\frac{\partial \Phi}{\partial x_j}\right]}_{\text{Diffusion term}} + \underbrace{S_\Phi}_{\text{Net source term}}$$

| Equation | Φ | $\Gamma_{eff}$(exch. coeff.) | $S_\Phi$(net source) |
|---|---|---|---|
| Conservation of Mass for the Mixture | 1 | 0 | 0 |
| Equation of Mass Transfer for Species k | $\omega_k$ | $\rho_m D_{eff}$ | $R_k$ |
| Momentum Equations $u_i$ i=(1,2,3) | $u_i$ | $\mu_{eff}$ | $-\partial p/\partial x_i + \rho_m B_i + S_{u_i}$ |
| Energy Equation ( Enthalpy Form) | h | $\lambda_{eff}/c_{pm}$ | $Q'''$ |
| Energy Equation (Temperature Form) | T | $\lambda_{eff}/c_{pm}$ | $Q'''/c_{pm}$ |

**Tab. 4** *Generalized representation of transport equations*

Derivation of the governing equations of fluid motion can be found in (Batchelor, 1967). In these equation ($\omega_k$ is the species mass fraction for a given species k, $c_{pm}$ is constant-pressure specific heat, h is the enthalpy, p is the pressure, T is the temperature, $u_i$ is the velocity, $Q'''$ is internal heat generation rates, other terms will be illustrated later ), the suffix m refers to the fluid mixture. For a single component fluid, the suffix may be dropped and the equation of mass transfer becomes irrelevant. Similarly, the suffix eff indicates effective values of mass diffusivity D, viscosity μ, and thermal conductivity $\lambda$.In turbulent flows, however, the transport properties assume values much in excess of the values ascribed to the fluid; moreover, the effective transport properties turn out to be properties of the flow rather than those of the fluid. The rate of change (or time derivative)term is to be invoked only when a transient phenomenon is under consideration. The term $\rho_m \Phi$ denotes the amount of extensive property available in a unit volume. The convection (second) term accounts for transport of Φ due to bulk motion. This first-order derivative term is relatively uncomplicated but assumes considerable significance when stable and convergent numerical solutions are to be economically obtained. The greatest impediment to obtaining physically accurate solutions is offered by the diffusion and the net source (S ) terms because both these terms require empirical information. In laminar flows, the diffusion term represented by the second-order derivative offers no difficulty because Γ being a fluid property, can be accurately determined (via experiments) in isolation of the flow under consideration. In turbulent (or transitional) flows, however, determination of $\Gamma_{eff}$ requires considerable empirical support. This is named as turbulence modeling (see next chapter). Although turbulence models of adequate generality (at least, for specific classes of flows) have been proposed in literature. These models determine $\Gamma_{eff}$ from simple algebraic empirical laws. Sometimes, $\Gamma_{eff}$ is also determined from other scalar quantities (such as turbulent kinetic energy and/or its dissipation rate) for which differential equations are constituted. Fortunately, these equations often have the form of transport equation. The term net source implies an algebraic sum of sources and sinks of Φ. Thus, in a chemically reacting flow (combustion, for example), a given species k maybe generated via some chemical reactions and destroyed (or consumed) via some others and $R_k$will comprise both positive and negative contributions. Also, some chemical

reactions may be exothermic, endothermic, making positive and negative contributions to Q‴. Similarly, the term $B_i$ in the momentum equations may represent a buoyancy force, a centrifugal and/or Coriolis force, an electromagnetic force, etc. Sometimes, $B_i$ may also represent resistance forces. Thus, in a mixture of gas and solid particles, Bi will represent the drag offered by the particles on air, or, in a fluid flow through a densely filled medium. Such empirical resistance laws are often determined from experiments or modeled numerically. The terms $S_{u_i}$ represent viscous terms arising from Stokes's stress laws. For static solid domains the conservation of energy equation can account for heat transport due to solid motion, conduction, and volumetric heat sources:

$$\frac{\partial(\rho_s \Phi)}{\partial t} = \frac{\partial}{\partial x_j}\left[\lambda_s \frac{\partial T}{\partial x_j}\right] + Q_s'''$$

where$\rho_s$ and $\lambda_s$ are the density, and thermal conductivity of the solid and $Q_s'''$is an volumetric heat source. The transport equations described above must be extended with constitutive equations of state for density and for enthalpy. In the most general case, these state equations have the form:

$$\rho = \rho(p,T)$$

$$dh = \left.\frac{\partial h}{dT}\right|_p dT + \left.\frac{\partial h}{dp}\right|_T dp = c_p dT + \left.\frac{\partial h}{dp}\right|_T dp$$

$$c_p = c_p(p,T)$$

The standard Redlich Kwong real gas is used because is considered one of the most accurate. The equations of state are written as:

$$p = \frac{RT}{v - \frac{0.08664RT_c}{p_c}} - \frac{\frac{0.42747R^2T_c^2}{p_c}\left(\frac{T}{T_c}\right)^{-0.5}}{v\left(v + \frac{0.08664RT_c}{p_c}\right)}$$

where $v$ is the specific volume and $p_c$,$T_c$ are critical pressure and temperature. In order to provide a full description of the gas properties, the flow solver must also calculate enthalpy and entropy(ideal gas state assumed as reference state):

$$h(T,v) = \underbrace{\int_{v_{ref}}^{\infty}\left(T\left(\frac{dp}{dT}\right)_v - p\right)dv_{Tref} + \int_{T_{ref}}^{T} c_{v0}\,dT - \int_{v}^{\infty}\left(T\left(\frac{dp}{dT}\right)_v - p\right)dv_T + e(T_{ref}, v_{ref})}_{e(p,T)} + pv$$

$$s(T,v) = \int_{v_{ref}}^{\infty}\left(\frac{dp}{dT}\right)_v dv_{Tref} + \int_{T_{ref}}^{T}\frac{c_{p0}}{T}dT - R\ln\left(\frac{p}{p_{ref}}\right) - \int_{v}^{\infty}\left(\frac{dp}{dT}\right)_v dv_T + s(T_{ref}, v_{ref})$$

Where$c_{V0}$ and $c_{p0}$ are the zero pressure ideal gas specific heat capacity. Other properties, such as the specific heat capacity at constant volume, can be evaluated from the internal energy:

$$c_v = \left(\frac{\partial u}{\partial T}\right)_v = \frac{\partial \int_{T_{ref}}^{T}(c_{p0}(T) - R)dT}{\partial T} - \frac{2\frac{0.42747R^2T_c^2}{p_c}\left(\frac{T}{T_c}\right)^{-0.5}}{\frac{0.08664RT_c}{p_c}T}\log\left(1 + \frac{\frac{0.08664RT_c}{p_c}}{v}\right)$$

The specific heat capacity at constant pressure$c_p$is calculated from $c_v$ using:

$$c_p = c_v + vT\frac{\left(-\frac{\left(\frac{\partial p}{\partial T}\right)_v}{v\left(\frac{\partial p}{\partial v}\right)_T}\right)^2}{-\frac{1}{v\left(\frac{\partial p}{\partial v}\right)_T}}$$

Unfortunately in ANSYS-CFX it is not possible to couple particles with gases that use the real gas equations of state. For the dust mobilization preliminary model a simple ideal gas model is used.

### V.III THREE-DIMENSIONAL DOMAIN DISCRETIZATION

Safety analysis related to pressurization of vessels are modeled with a rather coarse discretization including about $10^3$ mesh points. However some safety issues were clearly identified where a much finer resolution of the simulation tools was required. These issues are often related to situations where the 3D aspects of the flow and the geometrical effects have a significant influence. Turbulence and dust mobilization is a common feature of these flows. CFD tools are then required which may model small scale mixing phenomena with a fine space resolution including $10^5$ to$10^7$ mesh points. Care was taken to correctly mesh the domain with structured grids. A 3D axial-symmetric domain was considered in performing the CFD simulations, as shown in **Errore. L'origine riferimento non è stata trovata.** where the cartesian coordinate reference system is also reported. The spatial discretization consists of hexahedral elements both for the vessel domain and the horizontal inlet pipe. The 3D axial-symmetric domain was discretized using three structured grids (see **Errore. L'origine riferimento non è stata trovata.**).The number of cells used to mesh the STARDUST vessel and the inlet region are summarized in **Errore. L'origine riferimento non è stata trovata.**. The first grid (Coarse) was a mesh of 22.644 cells and radially refined only near the inlet axis of the domain to accurately solve the flow and the temperature distribution in these regions. The second grid (Fine) was a structured mesh of 249.084 cells. For LES, the computational grid must be chosen such that the separation of the resolved and the subgrid-scales occurs in the inertial subrange of the energy spectrum. Accordingly, the Fine grid size has been chosen to be one order of magnitude larger than that of the smallest scales (Kolmogorov scale) following Mukunda et al.(Mukunda, 1992).The third grid (Extra Fine) was a mesh of 2.264.402 cells radially refined both near the axis and near the

lateral wall. Grids were generated with an automatic procedure programmed in Gambit pre-processor.

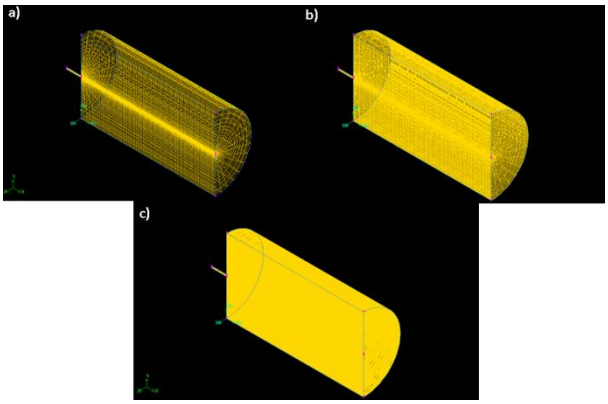


**Fig.11** *Structured grid a)Coarse, b) Fine and c) Ext. Fine*

| Grid dimension | |
|---|---|
| Name | Number of cells |
| Coarse | 22.644 |
| Fine | 249.084 |
| Ext. Fine | 2.264.402 |

**Tab. 5** *Grid dimension*

The three-dimensional grid is generated by extrusion from a bi-dimensional grid that contains inlet hole on its surface.

V.IV RESULTS

In the setup module of ASYS-CFX, the fluid flow simulation parameters and boundary conditions were explicitly specified. The fluid domain and the different boundary conditions imposed are the same of model development phase but now the external air enters into the vessel with a fixed flow rate according to the desired constant pressurization rate. On the basis of the available experimental data concerning the inlet flow rate inlet function can be simplified, with a conservative approximation, in a linear increase of the pressurization rate for the first second of the transient and a constant pressurization rate for the remaining transient (**Errore. L'origine riferimento non è stata trovata.**).This for to take into account the time necessary for the opening of the inlet valve and the time necessary to reach the regime of the mass flow rate.

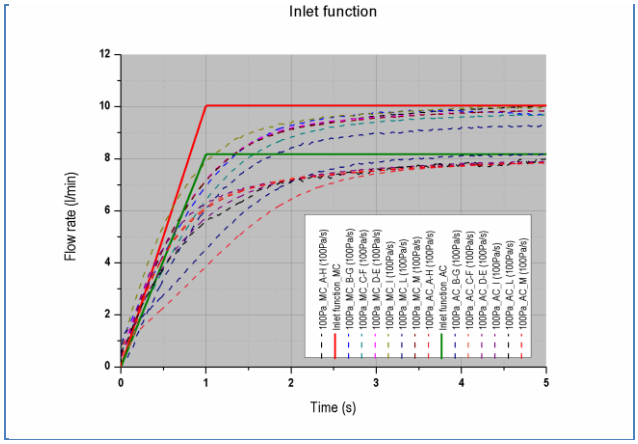


**Fig.12** *Air flow rate time trend imposed as inlet boundary condition (Inlet function)*

The inlet air temperature is set to the environmental value (T=296K). No-slip boundary conditions were assumed at all the walls. All the walls, except for the heated wall both in MC and AC experiment were a temperature condition is set up, the model includes the effect of heat transfer through the walls with the environment as previously discussed for the development of CFD model. The condition of the environment is equal to T=296 K and P=101325 Pa (ambient condition). The heated wall temperatures are maintained for both cases constant at fixed temperature both for MC (Twall=25°C) and AC (Twall=110°C) during the whole transient. As internal initial conditions, two different initial condition, 100 and 1000 Pa, were considered in order to verify the effect of pressure on the velocity during the transient. The exact value of initial internal condition (due to the experimental difficulty of setting the internal pressure and temperature at the set point value) are provided by STARDUST data The operating fluid used in the simulations was dry air assumed initially at rest. The density of the fluid was evaluated using the standard Redlich Kwong real gas and the other thermodynamic properties were considered variable according to internal database. The operating fluid used in the simulations was dry air assumed initially at rest.

In present section experimental results, with a frequency of 2 Hz (acquisition stops at 9500 Pa), inside the STARDUST vessel are compared to those provided by the simulations obtained with the ANSYS-CFX code and with the analytic unsteady solution of pressurization process (only for model development phase).

Preliminary analysis of experimental show that there is no relevant difference between the AC experiment with an internal pressure of 100 and 1000 Pa. Numerical and experimental results for 100Pa test, both in MC and AC, at different pressurization will be discussed because are considered most relevant for the validation case.

For the MC cases the average temperature increases from environment temperature (294 K) to 328 K (11%) in about 22 s. For the AC cases the average temperature decreases from initial internal temperature (384 K) to 305 K (12%) in about 18 s. Results appear to be concordant, as simulations satisfactorily reproduce experimental results only for MC case. Agreement seems to be poor for AC case. Figure 13 shows the calculated temperature field inside the domain.

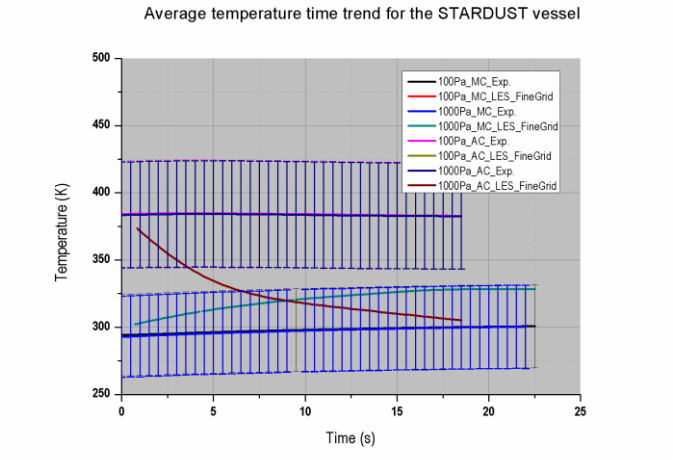


**Fig.13***: Numeric average temperature time trend for the STARDUST vessel*

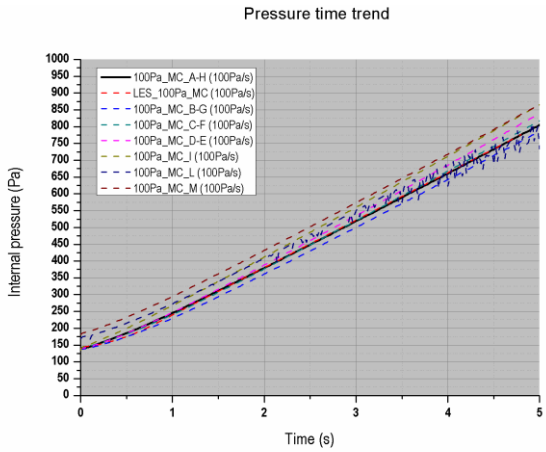


**Fig.14**: *Average pressure time trend*

This poor agreement may be caused by thermal high thermal inertia of TJ thermocouple. The effect of wall temperature and initial internal pressure on pressurization rate and filling time is summarized in Table 6.

| Effect of wall temperature and initial internal pressure on pressurization rate | | | |
|---|---|---|---|
| **Effect** | **Experimental** | **Analytic** | **Numeric** |
| Internal pressure | 4,69% | Insensible | 4,74% |
| Wall temperature | 16,12% | 23,62% | 16,49% |
| **Effect of wall temperature and initial internal pressure on filling time** | | | |
| **Effect** | **Experimental** | **Analytic** | **Numeric** |
| Internal pressure | -2,22% | -1,08% | 1,81% |
| Wall temperature | -17,78% | -12,94% | -19,11% |

**Tab. 6**: *Effect of wall temperature and initial internal pressure on pressurization rate and filling time*

Global results comparison gives significant indications: The wall temperature, and then the internal one, play an important role in the LOVA CFD simulation even more than the initial internal pressure variation.
For the LOVA simulation, consistently with the air flux at the inlet of the domain, set as mentioned, the obtained difference of average pressure, $\Delta P(t)$, inside the vessel shows, as required, a linear trend after with required slope for all simulation. In Figure 14 the comparison between calculated and experimental both for MC and AC case. Measurements of the gas velocity in the free jet were carried out using both pressure near-field dynamic transducers.

The axial velocity evaluated close to the air injection increases from zero to the maximum in the first second and then decreases. The CFD applications show stable numerical results for modeling local gas velocity field at low pressure conditions. The calculated data show a satisfying global agreement with experimental data for all performed experiments and simulation(from 1/3 to 2/3 of the vessel about 33%) .The high axial velocity region close to the air inlet corresponds to the expansion jet flow area.
The calculations show that the air velocities always increase when the vessel is heated (AC).The air velocity reaches its peak value, 770m/s for 100 Pa/s AC case , at about 0.7s. This is a negative result from the safety view point because an accident during the normal operation a typical temperature ranges of the plants can mobilize a higher amount of dust. If the temperature of the air becomes higher, air density becomes lower, which would create a higher air velocity in the vessel. However, with the increase of the temperature the viscosity of the gas increases and the pressure loss is proportional to the velocity squared. In other words, the resistance increases much slower than the density reduction with the increase of the average temperature. The net effect is a reduction in air ingress velocity with higher temperature.
It was possible to compare the temperatures obtained by LES with the temperatures measured inside the STARDUST vessel. No increase is detected by the thermocouples in experiments during the whole pressurization transient. In order to explain better the average temperature time trend shown in Figure 15, we assumed valid the adiabatic unsteady analytical model again. Figure 15 shows the average temperature trend obtained from adiabatic unsteady model compared to the data calculated with ASYS-CFX code. Analytical data agree well with the CFD results and both the trends show how temperature increases because the flow work, associated with the pressure at the inlet section, was converted in internal energy (Final temperature is about $T_{\_final} \approx \gamma T_{\_initial}$). Data calculated using LES for point A, placed very close to the inlet section and then near the expansion zone showing a sharp drop in the first second of simulation with a minimum of about 130 K after that temperature increases.

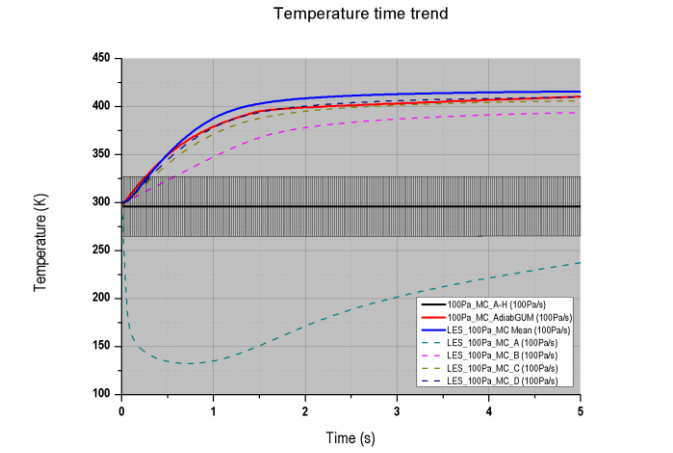


**Fig.15** *Temperature time trend*

## VI. CONCLUSION

For all the experiments is it possible observe that :

- the velocity values measured by PT 455 on the central line decrease of 20-25% passing from position near air inlet to the lid;
- the velocity values measured by PT 461 on the central line increase of 20-25% passing from position near air inlet to the lid;
- At the same distances from the valve the maximum velocity values measured on the central line are almost 20% higher than the the ones measured on the other lines;
- The maximum velocity values measured on the same point by the same PT are almost 15-20 % higher in case of hot experiments (in operative conditions).
- The maximum velocity values are measure almost between the time of 1s and 2s in accordance with other experimental campaigns and simulations [5,6,7,8,9,10];
- The initial pressure inside the chamber (100 Pa or 1000 Pa) doesn't influence critically the maximum velocity values measured.
- The calculated data show a satisfying global agreement with experimental data for all performed experiments and simulation;
- The wall temperature, and then the internal one, play an important role in the LOVA CFD simulation even more than the initial internal pressure variation;
- The net effect is a reduction in air ingress velocity with higher temperature.

## VII. BIBLIOGRAPHY

[1] C. Bellecci, P. Gaudio, I. Lupelli, A. Malizia, M.T. Porfiri, M. Richetta. Dust mobilization and transport measures in the STARDUST facility, EPS2008 Proceedings, 35th EPS Conference on Plasma Phys. Hersonissos, 9 - 13 June 2008 ECA Vol.32, P-1.175 (2008). (http://epsppd.epfl.ch/Hersonissos/pdf/P1_175.pdf)

[2] M.T. Porfiri, N. Forgione, S. Paci, A. Rufoloni, Dust mobilization experiments in the context of the fusion plants – STARDUST facility, Fusion Engineering and Design 81 (2006) 1353-1358.

[3] E. Eberta, J. Raeder, LOCA, LOFA and LOVA analyses pertaining to NET/ITER safety design guidance, Fusion Engineering and Design 17, (1991) Pages 307-312.

[4] ITER-JCT Generic Site Safety Report N84 Garching (Germany), July 2001

[5] C Bellecci, P Gaudio, I Lupelli, A Malizia, M T Porfiri, R Quaranta, M Richetta, "STARDUST experimental campaign and numerical simulations: Influence of obstacles and temperature on dust resuspension in a Vacuum Vessel under LOVA", Nuclear Fusion, IOPscience, 2010, Nucl. Fusion 51 (2011) 053017, 27/04/2011 (http://stacks.iop.org/0029-5515/51/053017)

[6] C Bellecci, P Gaudio, I Lupelli, A Malizia, M T Porfiri, R Quaranta, M Richetta, "Loss of Vacuum Accident (LOVA): Comparison of Computational Fluid Dynamics (CFD) flow velocities against experimental data for the model validation", Fusion Engineering and Design, Elsevier, 2010, publication on-line complete (http://dx.doi.org/10.1016/j.fusengdes.2011.02.057).

[7] P Gaudio, A Malizia, I Lupelli, "RNG k-ε modelling and mobilization experiments of loss of vacuum in small tanks for nuclear fusion safety applications", International Journal of Systems Engineering, Applications and Development, WSEAS, ISSN:2074-1308, Issue 1, Volume 5, 2001 (pag.287-305).

[10] P.Gaudio, A.Malizia, I.Lupelli, "Experimental and Numerical Analysis of Dust Resuspension for Supporting Chemical and Radiological Risk Assessment in a Nuclear Fusion Device" "International Conference on Mathematical Models for Engineering Science (MMES' 10), Puerto De La Cruz, Tenerife, November 30- December 2, 2010, ISBN 978-960-474-252-3, Electronic Version ISSN: 1792-684X, pag. 134-147.